Neuroimaging abnormalities in clade C HIV are independent of Tat genetic diversity

Robert H. Paul[1], **Sarah Phillips**[1], **Jacqueline Hoare**[2], **David H. Laidlaw**[3], **Ryan Cabeen**[3], **Gayla R. Olbricht**[4], **Yuqing Su**[4], **Dan J. Stein**[2], **Susan Engelbrecht**[5], **Soraya Seedat**[6], **Lauren E. Salminen**[7], **Laurie M. Baker**[1], **Jodi Heaps**[1], and **John Joska**[2]

[1] Missouri Institute of Mental Health, University of Missouri, St. Louis, MO, USA

[2] Department of Psychiatry and Mental Health, University of Cape Town, Cape Town 7700, South Africa

[3] Department of Computer Science, Brown University, Providence, RI 02912, USA

[4] Department of Mathematics and Statistics, Missouri University of Science and Technology, Rolla, MO 65409, USA

[5] Division of Medical Virology, Stellenbosch University and National Health Laboratory Services (NHLS), Cape Town, South Africa

[6] MRC Unit on Anxiety and Stress Disorders, Department of Psychiatry, University of Stellenbosch, Stellenbosch 7599, South Africa

[7] Mark and Mary Stevens Neuroimaging and Informatics Institute, University of Southern California, Los Angeles, CA 90007, USA

Abstract

Controversy remains regarding the neurotoxicity of clade C human immunodeficiency virus (HIV-C). When examined in preclinical studies, a cysteine to serine substitution in the C31 dicysteine motif of the HIV-C Tat protein (C31S) results in less severe brain injury compared to other viral clades. By contrast, patient cohort studies identify significant neuropsychological impairment among HIV-C individuals independent of Tat variability. The present study clarified this discrepancy by examining neuroimaging markers of brain integrity among HIV-C individuals with and without the Tat substitution. Thirty-seven HIV-C individuals with the Tat C31S substitution, 109 HIV-C individuals without the Tat substitution (C31C), and 34 HIV− controls underwent 3T structural magnetic resonance imaging (MRI) and diffusion tensor imaging (DTI). Volumes were determined for the caudate, putamen, thalamus, corpus callosum, total gray matter, and total white matter. DTI metrics included fractional anisotropy (FA), radial diffusivity (RD), and axial diffusivity (AD). Tracts of interest included the anterior thalamic radiation (ATR), cingulum bundle (CING), uncinate fasciculus (UNC), and corpus callosum (CC). HIV+ individuals exhibited smaller volumes in subcortical gray matter, total gray matter and total white matter

compared to HIV− controls. HIV+ individuals also exhibited DTI abnormalities across multiple tracts compared to HIV− controls. By contrast, neither volumetric nor diffusion indices differed significantly between the Tat C31S and C31C groups. Tat C31S status is not a sufficient biomarker of HIV-related brain integrity in patient populations. Clinical attention directed at brain health is warranted for all HIV+ individuals, independent of Tat C31S or clade C status.

Keywords

HIV; Clade C; C30C31 dicysteine motif; Tat C31S; Neuroimaging

Introduction

HIV viral clade has been identified as a possible moderator of HIV-related neurological outcomes (Rao et al. 2008; Sacktor et al. 2009; Mishra et al. 2008; Ranga et al. 2004). Approximately half of all global HIV infections are comprised of clade C (HIV-C; (Osmanov et al. 2002; McCutchan 2006) which is the predominant genetic strain in South Africa, India, and regions of both Brazil and China (Hemelaar et al. 2011). Multiple laboratory studies reveal lower neurovirulence associated with HIV-C compared to other clades such as clade B (HIV-B) (Rao et al. 2008; Mishra et al. 2008; Constantino et al. 2011), which is a neuropathogenic strain prevalent in North and South America, Australia, and Western Europe (Chan et al. 2014). The reduced neurovirulence of HIV-C has been attributed to a naturally occurring cysteine to serine substitution at position 31 (C31S) in the HIV-C Tat protein that is highly conserved in HIV-C (Rao et al. 2008; Mishra et al. 2008; Ranga et al. 2004). The Tat C31S substitution results in reduced monocyte chemotaxis, astrogliosis, pro-inflammatory cytokines, and neuronal damage when compared to assays using HIV-B with a C31C Tat motif (Rao et al. 2008; Gandhi et al. 2009). Behaviorally, mice injected with C31S perform better on memory tests compared to mice injected with C31C virus (Rao et al. 2008), revealing a functional benefit of the HIV-C Tat polymorphism.

However, results from clinical studies indicate that the cognitive phenotype of HIV-C is indistinguishable from HIV-B. For example, Montiero de Almeida et al. (de Almeida et al. 2013) revealed no significant differences in the frequency of mild, moderate, or severe cognitive impairment between HIV-C and HIV-B. This is consistent with multiple studies conducted in South Africa and India that describe significant cognitive impairment in HIV+ adults and children (Hoare et al. 2015a; Joska et al. 2011; Yepthomi et al. 2006; Gupta et al. 2007; Ghate et al. 2014). More recently, our group compared cognitive performances between HIV-C individuals with and without the Tat C31S polymorphism and reported no significant differences in the cognitive phenotype or severity of cognitive impairment by Tat status (Paul et al. 2014). These findings stand in contrast to laboratory studies reporting diminished neurovirulence in HIV-C and raise concern that individuals infected with the most common viral clade worldwide are equally vulnerable to HIV-related brain disruption as individuals infected with HIV-B.

One limitation of clinical studies conducted to date is the reliance on neuropsychological definitions of brain damage. Neuropsychological tests are potentially vulnerable to

confounding variables (e.g., cultural relevance, participant effort (Ostrosky-Solis et al. 2004; Rosselli & Ardila 2003)), and even under optimal conditions, these tests may lack the requisite sensitivity to detect the impact of Tat variability on the brain. Structural neuroimaging provides a sensitive and robust method to resolve these concerns. Chronically, infected HIV+ individuals typically exhibit smaller volumes of basal ganglia structures, total white matter, and total cortical gray matter on magnetic resonance imaging (MRI) when compared to HIV− controls (Ances et al. 2012; Hawkins et al. 1993; Heaps et al. 2012; Paul et al. 2002; Paul et al. 2008; Heaps et al. 2015). Further, recent data indicate that brain volumes decline over the course of HIV infection even in the context of viral suppression (Kallianpur et al. 2016), supporting the sensitivity of brain volume as a marker of disease pathogenesis.

Microstructural abnormalities in cerebral white matter are also commonly reported in HIV+ individuals. HIV is associated with reduced fractional anisotropy (FA) and increased mean diffusivity (MD) on diffusion tensor imaging (DTI) (Filippi et al. 2001; Gongvatana et al. 2009; Leite et al. 2013; Hoare et al. 2015b). Additional studies utilizing DTI reveal increased radial diffusivity (RD) and axial diffusivity (AD), suggesting damage to neuronal subcomponents including myelin and axonal integrity (respectively) in HIV+ individuals (Leite et al. 2013; Chen et al. 2009). Previous work using the nonhuman primate model of HIV revealed reduced FA within weeks of inoculation and prior to the expression of cognitive impairment (He et al. 2003), demonstrating the sensitivity of DTI to HIV-related brain disruption. Further, since structural MRI and DTI are not confounded by the same limitations inherent in neuropsychological testing (e.g., participant effort), the methods provide a robust approach to determine the relevance of the Tat C31S polymorphism in patient samples.

The present study examined the neurovirulence of the two HIV-C Tat variants (C31C and C31S) using structural MRI and DTI. Structural brain volumes and DTI fiber bundle tractography were examined in regions of interest (ROIs) commonly reported in the HIV literature (Fig. 1). We predicted that if present, the biological relevance of C31S would be defined by a unique neuroimaging signature on volumetric and diffusion indices.

Method

Participants

A total of 146 HIV+ individuals were recruited from primary care clinics in Cape Town and the Western Cape region of South Africa. HIV+ individuals included 37 individuals with HIV-C with the Tat C31S substitution, 109 HIV-C individuals without the Tat substitution (C31C), and 34 HIV− controls. HIV− controls were recruited from local Voluntary Counseling and Testing Clinics. Participation was voluntary and individuals were informed they could withdraw from the study at any time. Written informed consent was obtained following a thorough explanation of the study procedures. The methodological approach was approved by local University IRB committees. Individuals received financial compensation for their time.

Inclusion criteria included (1) Xhosa as the primary language and (2) Age 18 to 50 years. This age range was selected to avoid central nervous system (CNS) complications associated with neurodevelopment and advanced age (3) at least 5 years of formal education and (4) initiation of combination antiretroviral therapy (cART) within 3 months of enrollment for HIV+ individuals. Exclusion criteria included (1) major psychiatric conditions (schizophrenia, bipolar disorder, posttraumatic stress disorder, etc.), (2) neurological disease that could affect brain integrity (e.g., multiple sclerosis), (3) CDC stage A, (4) opportunistic infections of the CNS (e.g., cytomegalorvirus encephalitis, cryptococcal meningitis, toxoplasma encephalitis), (5) lifetime history of head injury resulting in loss of consciousness >30 min, and (6) current substance use disorder as determined by the Mini-International Neuropsychiatric Interview Plus (MINI Plus; (Sheehan et al. 1998)).

HIV-1 viral load and CD4+ cell counts

EDTA blood samples were collected and plasma and cell aliquots were stored at −70 °C. RNA was isolated from samples using the Abbott RealTime HIV-1 amplification reagent kit. Viral load was determined using the Abbott m2000sp and the Abbott m2000rt analysers (Abbott laboratories, Abbott Park, Illinois, USA). Analyses of CD4 cell count were completed on a FACSCalibur flow cytometer using MultiSET V1.1.2 software (BD Biosciences, San Jose, CA, USA).

PCR amplification and sequencing of Tat exon 1

We amplified the Tat exon 1 region (HXB2 position 5831–6045) by polymerase chain reaction (PCR) using the Promega GoTaq Flexi Kit (Promega, Madison, WI). The primer pair, TAT-1_OF (5′-AAAGCCACCTYTGCCTAG) / TAT-1_OR (5′-CTCATTGCCACTGTCTTCTGC), and TAT-1_IF (5′-GTAGARGATMGATGGAACRA) / TAT-1_IR (5′-CYCTAATTCTTTYAAYTAACC) were used for pre-nested and nested PCR, respectively. Both pre-nested and nested amplification reactions were held at 94 °C for 2 min, followed by 40 cycles of denaturing (94 °C; 30 s), annealing (55 °C; 30 s), and extension (72 °C; 1 min) followed by a final extension step for 7 min at 72 °C. The PCR product was kept at 4 °C until visualized using agarose gel electrophoresis.

To purify the PCR products, single-stranded DNA and diphosphates were degraded using Exonuclease 1 (Exo1) and Shrimp alkaline phosphatase (Amersham Pharmacia Biotech., NJ), respectively. All PCR products were sequenced on both strands using the BigDye Terminator Cycle Sequencing Ready Reaction Kit and analyzed on an ABI Prism 3130xl automated DNA sequencer (Applied Biosystems, Foster City, CA). Sequences were analyzed and the overlapping DNA fragments were assembled using Sequencher version 4.8 (Gene Codes Corporation, Ann Arbor, MI). Nucleotide sequences were translated into amino acid sequences and the C30C31 motif or C31S mutation was recorded. The Tat exon 1 subtype was determined using online subtyping tools COMET (http://comet.retrovirology.lu/) and jpHMM (http://jphmm.gobics.de/).

Neuroimaging acquisition

Imaging was acquired on a 3T Siemens Allegra scanner (Siemens AG, Erlangen Germany), with a 4-channel phased-array head coil. A customized single-shot multi-slice echo-planar

tensor-encoded imaging sequence was used to acquire 30 unique diffusion gradient directions that were repeated to give a total of 60 diffusion-weighted volumes. All 30 gradients were acquired at $b = 1000$ s/mm^2. Six baseline images were acquired and interleaved in the diffusion-weighted scans for motion-correction. Seventy contiguous slices were obtained per contrast with a 128×128 matrix and field of view (FOV) of 218×218 mm^3 (isotropic $1.7 \times 1.7 \times 1.7$ mm^3 voxels); TR 10 s, TE 103 ms using a full-Fourier transform. We also acquired a T1-weighted 3-dimensional magnetization-prepared rapid acquisition gradient echo (MP-RAGE) sequence [time of repetition (TR) = 2400 ms, echo time (TE = 2.38 ms), inversion time (TI) = 1000 ms, flip angle = 8 degrees, 162 slices, and voxel size = $1 \times 1 \times 1$ mm^3 for volumetric analyses (Fig. 2).

Volumetric analysis

Freesurfer software suite (v5.1) (Martinos Center, Harvard University, Boston, MA, USA; http://surfer.nmr.mgh.harvard.edu) was utilized for volumetric quantification. Briefly, MP-RAGE scans were transformed into a template space with the skull stripped and the brain segmented into white matter, gray matter, and ventricles. Brain regions were parcellated into subcortical and cortical ROIs using a surface deformation program (Fischl et al. 2002; Fischl & Dale 2000; Desikan et al. 2006). Images from all subjects were aligned to a common atlas (MNI305) (Fischl et al. 2002). ROIs in the present study included the caudate, putamen, thalamus, corpus callosum, total gray matter, and total white matter. Previous studies identify these ROIs are impacted by HIV neuropathogenesis (Heaps et al. 2012; Heaps et al. 2015; Kallianpur et al. 2013; Ortega et al. 2013). Volumes were measured bilaterally and then aggregated across hemispheres to form a composite measure for each ROI. Total intracranial volume (TICV) was utilized as a covariate in the general linear regression models.

Diffusion metrics

Diffusion-weighted images (DWIs) were preprocessed using FSL 5.0 (Jenkinson et al. 2012) as follows. DWIs were corrected for motion and eddy-current induced artifacts through affine registration to the first baseline volume using FSL FLIRT (Jenkinson & Smith 2001) with the mutual information criteria. The orientations of the gradient encoding directions were corrected by the rotation induced by these registrations (Leemans & Jones 2009), and the brain tissue was extracted using FSL brain extraction tool (BET) (Smith 2002) with a fraction threshold of 0.45. Diffusion tensor images were estimated for each subject using FSL DTIFIT.

Following this, a study-specific white matter atlas was created using DTI-TK (Zhang et al. 2007). The template diffusion tensor image was computed by iteratively deforming and averaging the population imaging data using the tensor-based deformable registration algorithm in DTI-TK (Zhang et al. 2006) with finite strain tensor reorientation and the deviatoric tensor similarity metric. This template was used to define inclusion and exclusion ROI masks for the anterior thalamic radiation (ATR), cingulum bundle (CING), uncinate fasciculus (UNC), and corpus callosum (CC) (Mori & van Zijl 2002). Whole brain tractography was performed in the template image, and subsets of curves were interactively selected to represent each tract-of-interest (TOI). For each bundle, two inclusion ROI masks

and one exclusion ROI mask were drawn in template space using ITK-SNAP (Yushkevich et al. 2006). These masks were placed at opposite ends of each tractography bundle template and drawn in reference to standard white matter atlases (Catani & de Schotten 2012; Oishi et al. 2010).

Subject-specific fiber bundle metrics were computed as follows. First, the TOI inclusion and exclusion masks were deformed to subject native space using the DTI-TK registration. Whole brain tractography was then performed in subject native space and a subset of curves in the TOI was selected using the two inclusion and exclusion masks. Tractography was performed using deterministic streamline integration (Zhang & Laidlaw 2003) with a step size of 1 mm, tricubic interpolation, and four jittered seeds per voxel. Termination criteria included an angle threshold of 45 degrees and minimum FA of 0.15. Fiber curves with a length less than 10 mm were excluded from the analysis. The following bundle-average metrics were computed from the resulting curves and retained for statistical analyses: FA, MD, RD, and AD (Correia et al. 2008), averaged across hemispheres.

Neuroimaging quality control

The MR images were each visually inspected for artifact, proper positioning within the field of view, and motion/noise abnormalities across subjects. The quality of the MP-RAGE analysis was assessed by reviewing Freesurfer pipeline logs and segmentation results. Eighteen subjects were excluded from the MP-RAGE pipeline because the Freesurfer pipeline failed before completion. Seven subjects were excluded from the diffusion MR image analysis because either no diffusion scan was acquired or a major artifact was present. The quality of the diffusion MRI registration was assessed by reviewing FA maps superimposed on the population average FA map. The quality of the fiber bundle reconstructions was assessed by 3D visualization of the curve data to check for erroneous fibers.

Statistical analyses

Demographic variables were first compared between groups of HIV patients using independent two-sample t tests (age, education) and chi-square tests (sex). For the C31S and the C31C groups, t tests were conducted to compare average CD4 counts, $\log_{10}$ viral load, duration of infection (in months), and self-reported depression using the CES-D (Radloff 1977). Chi-square tests were used to compare the percentage of individuals with detectable viral load and percentage of individuals on cART between the C31S and C31C groups. Demographic variables that differed significantly between groups were considered as covariates in the primary analyses. The first set of primary analyses tested neuroimaging differences between HIV+ and HIV− individuals using multivariate analysis of variance/covariance (MANOVA/MANCOVA) models. Separate MANOVAs/MANCOVAs were fit for DTI and volumetric variables due to the differential sensitivity of the two outcomes on brain integrity. These analyses were repeated to compare C31S and C31C individuals. Assumptions of MANOVA/MANCOVA were investigated in all analyses, including normality, linearity, homogenous covariance matrices, multicollinearity, outlier checking, and no interaction (MANCOVA only). Assumptions were met unless otherwise noted in subsequent results. Following significance of a group effect in the multivariate model,

univariate analyses were employed to determine which dependent variables differed significantly between groups. The false discovery rate (FDR) was controlled at 0.05 to correct for the multiple comparisons.

Results

Demographic characteristics

Descriptive statistics for demographic variables are reported in Table 1. HIV+ individuals (n = 146) differed significantly from HIV− individuals (n = 34) on average years of age (t = 6.32, $p < 0.01$), years of education (t = −2.59, $p < 0.01$), and sex ($\chi^2(1)$ = 10.85, $p < 0.01$). Since the difference in average education level between groups was minimal (<1 year), education was not included as a covariate in subsequent analysis. Age and sex were included as covariates in the subsequent MANCOVA models for the HIV+ vs. HIV− comparison.

There were no significant differences between C31S (n = 37) or C31C (n = 109) groups with respect to age (t = −1.23, p = 0.22), years of education (t = −1.35, p = 0.10), and sex ($\chi^2(1)$ = 0.49, p = 0.48). Thus, age, years of education, and sex were not included as covariates in subsequent models for the C31S vs. C31C comparison. For DTI metrics, MANOVA models were employed since no covariates were included, whereas TICV was included as a covariate in a MANCOVA model for volumetric indices. Additionally, the HIV-C Tat C31S and C31C groups did not differ significantly in $\log_{10}$ viral load (t = 0.18, p = 0.85), average CD4 count (t = −0.1, p = 0.92), duration of infection (t = −0.35, p = 0.73), CES-D scores (t = 0.83, p = 0.41), percentage on cART ($\chi^2(1)$ = 1.14, p = 0.29), and percentage with detectable viral load ($\chi^2(1)$ = 1.04, p = 0.31). Note the sample sizes for the primarily analyses described in the following sections differ slightly than those reported in Table 1 because not all individuals had both structural MRI and DTI images. The overall results of the demographic analyses were not altered when the analyses were restricted to individuals with both scans.

Volumetrics between HIV+ and HIV− individuals

Volumetric data were available for 128 HIV+ and 29 HIV− individuals. Multicollinearity was not an issue for the volumetric data, as none of the pairwise correlations between the ROIs exceeded r = 0.70 (Table 2). Results of the MANCOVA revealed a significant difference in brain volumes between HIV+ and HIV− individuals (Wilk's Λ = 0.78, F(6,147) = 6.71, $p < 0.01$). Results of the adjusted analyses revealed significantly smaller volumes among HIV+ individuals in the caudate, putamen, thalamus, total gray matter, and total white matter compared to the HIV− individuals. Significant differences were not observed in the CC after applying the FDR correction (Table 3).

DTI differences between HIV+ and HIV− individuals

DTI data were available for 137 HIV+ and 24 HIV− individuals. Pairwise Pearson's correlations between RD, AD, MD, and FA indicated that MD was highly correlated ($r >$ 0.90) with AD and RD in all TOIs, and therefore, MD was dropped from the analysis due to its redundancy and multicollinearity. Similarly, AD was highly correlated ($r >$ 0.90) with RD in the ATR and UNC tracts only and was dropped from those analyses. Results of the

MANCOVAs revealed a significant difference between the HIV+ and HIV− groups on DTI metrics for the CC (Wilk's $\Lambda = 0.948$, $F(3,155) = 2.81$, $p < 0.05$), ATR (Wilk's $\Lambda = 0.94$, $F(2,156) = 4.40$, $p < 0.05$), and UNC (Wilk's $\Lambda = 0.85$, $F(2,156) = 12.95$, $p < 0.01$). Univariate analysis revealed significant differences in AD and RD for the CC, RD for the ATR, and both FA and RD for the UNC after controlling for multiple comparisons (Table 2). A trend was noted between the HIV+ and HIV− groups on the DTI metrics for the CING (Wilk's $\Lambda = 0.953$, $F(3,155) = 2.56$, $p = 0.05$), with the univariate analysis revealing higher RD and AD in the HIV+ individuals compared to HIV− controls.

Volumetric differences between C31S and C31C individuals

Volumetric data were available for 34 C31S and 94 C31C individuals. Multicollinearity was not an issue for the volumetric data, as none of the pairwise correlations between the ROIs exceeded $r = 0.70$. Results of the MANCOVA revealed no significant differences between the C31S and C31C groups on the volumetric variables (Wilk's $\Lambda = 0.97$, $F(6,120) = 0.52$, $p = 0.78$). Univariate results are given in Table 5.

DTI differences between C31S and C31C individuals

DTI data were available for 35 C31S and 102 C31C individuals. Similar to the previous analyses, MD was significantly correlated with the other diffusivity metrics and therefore, MD was dropped from the analysis. Similarly, AD was highly correlated ($r > 0.9$) with RD in the ATR and UNC tracts only and was dropped from those analyses. Results of the MANOVAs revealed no significant differences between the C31S and C31C groups on the DTI metrics for the CC (Wilk's $\Lambda = 0.967$, $F(3,133) = 1.51$, $p = 0.22$), CING (Wilk's $\Lambda = 0.991$, $F(3,133) = 0.38$, $p = 0.7$), ATR (Wilk's $\Lambda = 0.974$, $F(2,134) = 1.80$, $p = 0.1$), and UNC (Wilk's $\Lambda = 0.999$, $F(2,134) = 0.10$, $p = 0.9$). Univariate results are given in Table 4.

Relationships between clinical variables and imaging metrics

Pearson's correlations were calculated to examine relationships between the imaging metrics and duration of infection, CESD, CD4 count and $\log_{10}$ viral load within all HIV+ individuals, as well as separately for the C31S and C31C groups. Almost all correlations were less than 0.3, with no significant linear associations between the clinical and imaging variables. The only significant correlations were in the C31S group between CD4 count and total white matter ($r = -0.43$, p value = 0.01), and between $\log_{10}$ viral load and FA ($r = -0.40$, p value = 0.01) in the ATR (Table 5).

Discussion

The present study clarifies the controversy regarding the impact of the HIV-C Tat C31S substitution on brain integrity. We did not observe a unique signature of brain disruption associated with Tat C31S. When collapsed across Tat status, the HIV+ group exhibited significantly smaller brain volumes and greater white matter microstructural abnormalities compared to the HIV− group. Evidence of a main effect of HIV on brain imaging provides confidence that the absence of a unique contribution of the Tat C31S variant to brain structure was not due to confounds related to the sample or the imaging metrics. Similarly, power was sufficient to detect meaningful group differences, and therefore, the absence of a

Tat-specific imaging signature was not driven by sample sizes. Collectively, our findings provide compelling evidence that HIV-C is sufficiently neurovirulent to damage both gray and white matter brain regions.

Results from the present study are consistent with previous neuroimaging studies of adult and pediatric HIV patients conducted in South Africa where HIV-C is prevalent. Heaps et al. (Heaps et al. 2012) reported reduced volumes of the thalamus, total gray matter, and total white matter in HIV+ adults residing in South Africa compared to local HIV– controls. A follow-up comparison of HIV-C and HIV-B patients demonstrated no significant differences in the neuroimaging signatures related to clade diversity (Ortega et al. 2013). Other work from Hoare et al. (Hoare et al. 2011) revealed lower FA and higher MD in multiple white matter tracts of HIV+ adults from South Africa compared to seronegative controls. Further, South African children infected with perinatal HIV exhibit structural white matter damage (Hoare et al. 2015b; Ackermann et al. 2014; Hoare et al. 2012) and neuronal metabolite disruption in the basal ganglia (Mbugua et al. 2016). These neuroimaging abnormalities are present in children with vertically acquired disease despite initiation of cART during the first few months of life.

The present study is the first neuroimaging investigation conducted in South Africa where both HIV-C and Tat variance were confirmed with genetic sequencing. This methodological step is important as Rao et al. (Rao et al. 2013) reported variability in the conservation of the Tat polymorphism between India and South Africa. Specifically, while the frequency of C31S was less than 5% in samples from India, the frequency increased to more than 25% in samples from South Africa. Further, C31C variants isolated from South Africa triggered more monocyte chemotaxis, stimulated CCL2 induction, and damaged neuronal dendritic integrity compared to C31S isolates. Finally, mice injected with C31C isolates demonstrated more severe memory impairment compared to mice injected with C31S isolates and uninfected controls. These data align with outcomes from previous laboratory studies demonstrating less severe brain injury related to the Tat C31S polymorphism (Mishra et al. 2008; Ranga et al. 2004).

The lack of conservation of the C31S variant in South African isolates raises the possibility that previous reports of neuropsychological impairment in HIV-C among South African individuals were driven by the presence of the neurovirulent C31C Tat motif. However, our group recently reported no differences in the cognitive phenotype between individuals with C31C and individuals with C31S, suggesting that the Tat motif is not a primary driver of HIV-related brain dysfunction. Results from the current study demonstrate neuroimaging abnormalities regardless of the Tat C31S motif, indicating that the absence of cognitive variance related to the Tat polymorphism cannot be attributed to the reliance on neuropsychological tests to define brain integrity.

The extant literature is replete with evidence of cognitive impairment among children and adults with HIV from regions around the world with high frequency of clade C virus (de Almeida et al. 2013; Hoare et al. 2015a; Joska et al. 2011; Yepthomi et al. 2006; Gupta et al. 2007; Ghate et al. 2014; Paul et al. 2014; Hoare et al. 2015b). While most of these investigations did not sequence the dicysteine motif of Tat to confirm the presence of

cysteine or serine at position 31, the results are consistent with our previous cognitive study in which C31S status was defined (Paul et al. 2014). As such, while clade diversity moderates HIV-related brain dysfunction in controlled laboratory studies, these effects do not readily translate readily into patient outcomes. This is not surprising as a multiplex of host and viral factors influence neuroimaging and neuropsychological outcomes (Stern et al. 1996; Cohen et al. 2010; Jernigan et al. 2011; Gamaldo et al. 2013). A possible exception to the influence of clade on brain integrity is clade D (HIV-D) in Africa, which is associated with rapid immune depletion (Kiwanuka et al. 2010), early utilization of CXCR4 co-receptor tropism (Huang et al. 2007; Kaleebu et al. 2007), and faster disease progression (Kaleebu et al. 2002; Kiwanuka et al. 2008; Vasan et al. 2006). It remains unclear whether HIV-D individuals exhibit disproportional brain dysfunction compared to other clades and to what extent overall disease severity mediates brain outcomes in this population (Sacktor et al. 2009; Sacktor et al. 2014; Boivin et al. 2010).

It is important that future work continue to examine neuroimaging outcomes in patient cohorts to determine the viral and host factors that influence clinically relevant brain outcomes. Recent patient studies in Thailand, where clade AE recombinant is prevalent, reveal HIV RNA in the cerebrospinal fluid following acute exposure when clinical diagnostic assays for HIV are negative for p24 antigen and HIV antibody (Ananworanich et al. 2016; Valcour et al. 2012). Further, neuroimaging analyses demonstrate the evolution of subcortical brain atrophy even after 24 months of suppressive cART is initiated during the first weeks of HIV exposure (Kallianpur et al. 2016). Future studies are needed across clade subtypes to the key triggers of downstream immunological responses, seeding of viral reservoirs harbored in brain tissue or circulating monocytes, and plasma markers of immune activation.

A few limitations of the study merit attention. We utilized a cross-sectional design and as such, we cannot discuss the long-term trajectory of brain imaging outcomes associated with the Tat variants. Additionally, we did not examine other HIV viral proteins (e.g., Env, Nef, or gp120) and therefore, we cannot comment on the potential contribution of other viral proteins and disease mechanisms related to the neuroimaging outcomes. The sample size of the C31S genotype group ($n = 37$) was modest, though sufficient to detect at least a medium effect between groups. It is possible that a larger sample size would result in statistically significant differences between Tat genotype groups, though the clinical significance of a small effect would be unclear. Finally, HIV+ individuals in the current study had recently initiated cART, raising the possibility of opportunistic infections at the time of enrollment. However, we excluded individuals with medical comorbidities that could have confounded the results, and therefore, it is unlikely that the neuroimaging outcomes were negatively influenced by opportunistic infections.

In summary, results of the present study provide objective evidence of HIV-C neurovirulence independent of Tat diversity. The preponderance of data obtained from previous patient studies and the current study argue that Tat sequencing cannot be utilized as a prognostic marker of HIV-associated neurocognitive disorders or any measure of brain integrity related to HIV. As such, the estimated 20 million individuals infected with HIV-C worldwide are at risk for brain dysfunction and associated complications in overall health outcomes. Our

results accentuate the need to consider brain health in the clinical management of HIV, independent of viral clade or Tat variance.

Acknowledgments

References

Ackermann C, Andronikou S, Laughton B, Kidd M, Dobbels E, Innes S, et al. White matter signal abnormalities in children with suspected HIV-related neurologic disease on early combination antiretroviral therapy. Pediatr Infect Dis J. 2014; 33:e207–e212. [PubMed: 24595047]

Ananworanich J, Sacdalan CP, Pinyakorn S, Chomont N, de Souza M, Luekasemsuk T, et al. Virological and immunological characteristics of HIV-infected individuals at the earliest stage of infection. Journal of virus eradication. 2016; 2:43–48. [PubMed: 26889497]

Ances BM, Ortega M, Vaida F, Heaps J, Paul R. Independent effects of HIV, aging, and HAART on brain volumetric measures. Journal of acquired immune deficiency syndromes (1999). 2012; 59:469–477. [PubMed: 22269799]

Boivin MJ, Ruel TD, Boal HE, Bangirana P, Cao H, Eller LA, et al. HIV-subtype A is associated with poorer neuropsychological performance compared with subtype D in antiretroviral therapy-naive Ugandan children. AIDS. 2010; 24:1163–1170. [PubMed: 20425886]

Catani, M., de Schotten, MT. Atlas of human brain connections. 2012.

Chan PA, Reitsma MB, DeLong A, Boucek B, Nunn A, Salemi M, et al. Phylogenetic and geospatial evaluation of HIV-1 subtype diversity at the largest HIV center in Rhode Island. Infect Genet Evol. 2014; 28:358–366. [PubMed: 24721515]

Chen Y, An H, Zhu H, Stone T, Smith KJ, Hall C, et al. White matter abnormalities revealed by diffusion tensor imaging in non-demented and demented HIV+ patients. NeuroImage. 2009; 47:1154–1162. [PubMed: 19376246]

Cohen RA, Harezlak J, Schifitto G, Hana G, Clark U, Gongvatana A, et al. Effects of nadir CD4 count and duration of human immuno-deficiency virus infection on brain volumes in the highly active antiretroviral therapy era. J Neurovirol. 2010; 16:25–32. [PubMed: 20113183]

Constantino AA, Huang Y, Zhang H, Wood C, Zheng JC. HIV-1 clade B and C isolates exhibit differential replication: relevance to macrophage-mediated neurotoxicity. Neurotox Res. 2011; 20:277–288. [PubMed: 21336667]

Correia S, Lee SY, Voorn T, Tate DF, Paul RH, Zhang S, et al. Quantitative tractography metrics of white matter integrity in diffusion-tensor MRI. NeuroImage. 2008; 42:568–581. [PubMed: 18617421]

de Almeida S, Ribeiro C, de Pereira A, Badiee J, Cherner M, Smith D, et al. Neurocognitive impairment in HIV-1 clade C-versus B-infected individuals in Southern Brazil. Journal of NeuroVirology. 2013; 19:550–556. [PubMed: 24277437]

Desikan RS, Segonne F, Fischl B, Quinn BT, Dickerson BC, Blacker D, et al. An automated labeling system for subdividing the human cerebral cortex on MRI scans into gyral based regions of interest. NeuroImage. 2006; 31:968–980. [PubMed: 16530430]

Filippi CG, Ulug AM, Ryan E, Ferrando SJ, van Gorp W. Diffusion tensor imaging of patients with HIV and normal-appearing white matter on MR images of the brain. AJNR Am J Neuroradiol. 2001; 22:277–283. [PubMed: 11156769]

Fischl B, Dale AM. Measuring the thickness of the human cerebral cortex from magnetic resonance images. Proc Natl Acad Sci U S A. 2000; 97:11050–11055. [PubMed: 10984517]

Fischl B, Salat DH, Busa E, Albert M, Dieterich M, Haselgrove C, et al. Whole brain segmentation: automated labeling of neuroanatomical structures in the human brain. Neuron. 2002; 33:341–355. [PubMed: 11832223]

Gamaldo CE, Gamaldo A, Creighton J, Salas RE, Selnes OA, David PM, et al. Evaluating sleep and cognition in HIV. J Acquir Immune Defic Syndr. 2013; 63:609–616. [PubMed: 23722610]

Gandhi N, Saiyed Z, Thangavel S, Rodriguez J, Rao KV, Nair MP. Differential effects of HIV type 1 clade B and clade C Tat protein on expression of proinflammatory and antiinflammatory cytokines by primary monocytes. AIDS Res Hum Retrovir. 2009; 25:691–699. [PubMed: 19621989]

Ghate M, Narkhede H, Rahane G, Nirmalkar A, Gaikwad N, Kadam D. Cognitive function among HIV infected children in Pune. Indian J Pediatr. 2014; 82:515–518. [PubMed: 25432090]

Gongvatana A, Schweinsburg BC, Taylor MJ, Theilmann RJ, Letendre SL, Alhassoon OM, et al. White matter tract injury and cognitive impairment in human immunodeficiency virus–infected individuals. Journal of Neurovirology. 2009; 15:187–195. [PubMed: 19306228]

Gupta JD, Satishchandra P, Gopukumar K, Wilkie F, Waldrop-Valverde D, Ellis R, et al. Neuropsychological deficits in human immunodeficiency virus type 1 clade C-seropositive adults from South India. J Neurovirol. 2007; 13:195–202. [PubMed: 17613709]

Hawkins CP, McLaughlin JE, Kendall BE, McDonald WI. Pathological findings correlated with MRI in HIV infection. Neuroradiology. 1993; 35:264–268. [PubMed: 8388082]

He JGJ, Mui K, Aminipour S, Kim J, Fuller R, Rataj E, Lentz M, Sehgal P, Westmoreland S, de Crespigny A, Gonzalex R. Diffusion MR detection of early white matter changes in the SIV primate model of neuroaids. Intl Soc Mag Reson Med. 2003:2536.

Heaps JM, Joska J, Hoare J, Ortega M, Agrawal A, Seedat S, et al. Neuroimaging markers of human immunodeficiency virus infection in South Africa. Journal of NeuroVirology. 2012; 18:151–156. [PubMed: 22528474]

Heaps JM, Sithinamsuwan P, Paul R, Lerdlum S, Pothisri M, Clifford D, et al. Association between brain volumes and HAND in cART-naïve HIV+ individuals from Thailand. Journal of NeuroVirology. 2015; 21:105–112. [PubMed: 25604494]

Hemelaar J, Gouws E, Ghys PD, Osmanov S. Isolation W-UNfH, characterisation. Global trends in molecular epidemiology of HIV-1 during 2000–2007. AIDS. 2011; 25:679–689. [PubMed: 21297424]

Hoare J, Fouche J-P, Spottiswoode B, Sorsdahl K, Combrinck M, Stein DJ, et al. White-matter damage in clade C HIV-positive subjects: a diffusion tensor imaging study. The Journal of Neuropsychiatry and Clinical Neurosciences. 2011; 23:308315.

Hoare J, Fouche JP, Spottiswoode B, Donald K, Philipps N, Bezuidenhout H, et al. A diffusion tensor imaging and neurocognitive study of HIV-positive children who are HAART-naive Bslow progressors^. J Neurovirol. 2012; 18:205–212. [PubMed: 22552809]

Hoare J, Fouche J-P, Phillips N, Joska JA, Donald KA, Thomas K, et al. Clinical associations of white matter damage in cART-treated HIV-positive children in South Africa. Journal of NeuroVirology. 2015a; 21:120–128. [PubMed: 25604496]

Hoare J, Fouche J-P, Phillips N, Joska JA, Paul R, Donald KA, et al. White matter micro-structural changes in ART-naive and ART-treated children and adolescents infected with HIV in South Africa. AIDS. 2015b Publish Ahead of Print.

Huang W, Eshleman SH, Toma J, Fransen S, Stawiski E, Paxinos EE, et al. Coreceptor tropism in human immunodeficiency virus type 1 subtype D: high prevalence of CXCR4 tropism and heterogeneous composition of viral populations. J Virol. 2007; 81:7885–7893. [PubMed: 17507467]

Jenkinson M, Smith S. A global optimisation method for robust affine registration of brain images. Med Image Anal. 2001; 5:143–156. [PubMed: 11516708]

Jenkinson M, Beckmann CF, Behrens TE, Woolrich MW, Smith SM. FSL. NeuroImage. 2012; 62:782–790. [PubMed: 21979382]

Jernigan TL, Archibald SL, Fennema-Notestine C, Taylor MJ, Theilmann RJ, Julaton MD, et al. Clinical factors related to brain structure in HIV: the CHARTER study. J Neurovirol. 2011; 17:248–257. [PubMed: 21544705]

Joska JA, Westgarth-Taylor J, Myer L, Hoare J, Thomas KGF, Combrinck M, et al. Characterization of HIV-associated neurocognitive disorders among individuals starting antiretroviral therapy in South Africa. AIDS Behav. 2011; 15:1197–1203. [PubMed: 20614176]

Kaleebu P, French N, Mahe C, Yirrell D, Watera C, Lyagoba F, et al. Effect of human immunodeficiency virus (HIV) type 1 envelope subtypes A and D on disease progression in a large

cohort of HIV-1-positive persons in Uganda. The Journal of infectious diseases. 2002; 185:1244–1250. [PubMed: 12001041]

Kaleebu P, Nankya IL, Yirrell DL, Shafer LA, Kyosiimire-Lugemwa J, Lule DB, et al. Relation between chemokine receptor use, disease stage, and HIV-1 subtypes A and D: results from a rural Ugandan cohort. Journal of acquired immune deficiency syndromes (1999). 2007; 45:28–33. [PubMed: 17310935]

Kallianpur KJ, Shikuma C, Kirk GR, Shiramizu B, Valcour V, Chow D, et al. Peripheral blood HIV DNA is associated with atrophy of cerebellar and subcortical gray matter. Neurology. 2013; 80:1792–1799. [PubMed: 23596064]

Kallianpur, KJC., Jahanshad, Donn, Fletcher, Neda, Ananworanich, James L., Clifford, Jintanat, Benjapornpong, Katherine, Adams, Khunthalee, Spudich, Collin, Valcour, Serena S., Victor. for the The RV254/SEARCH010 Study Group. CROI. Boston, MA: 2016. Brain Volumetric Changes After 2 Years of ART Initiated During Acute HIV Infection | CROI Conference..

Kiwanuka N, Laeyendecker O, Robb M, Kigozi G, Arroyo M, McCutchan F, et al. Effect of human immunodeficiency virus Type 1 (HIV-1) subtype on disease progression in persons from Rakai, Uganda, with incident HIV-1 infection. The Journal of infectious diseases. 2008; 197:707–713. [PubMed: 18266607]

Kiwanuka N, Robb M, Laeyendecker O, Kigozi G, Wabwire-Mangen F, Makumbi FE, et al. HIV-1 viral subtype differences in the rate of CD4+ T-cell decline among HIV seroincident antiretroviral naive persons in Rakai district, Uganda. J Acquir Immune Defic Syndr. 2010; 54:180–184. [PubMed: 20010433]

Leemans A, Jones DK. The B-matrix must be rotated when correcting for subject motion in DTI data. Magn Reson Med. 2009; 61:1336–1349. [PubMed: 19319973]

Leite SCB, Corrêa DG, Doring TM, Kubo TTA, Netto TM, Ferracini R, et al. Diffusion tensor MRI evaluation of the corona radiata, cingulate gyri, and corpus callosum in HIV patients. Journal of magnetic resonance imaging: JMRI. 2013; 38:1488–1493. [PubMed: 23559497]

Mbugua KK, Holmes MJ, Cotton MF, Ratai EM, Little F, Hess AT, et al. HIV-associated CD4/8 depletion in infancy is associated with neurometabolic reductions in the basal ganglia at age 5 years despite early antiretroviral therapy. Aids. 2016

McCutchan FE. Global epidemiology of HIV. J Med Virol. 2006; 78(Suppl 1):S7–s12. [PubMed: 16622870]

Mishra M, Vetrivel S, Siddappa NB, Ranga U, Seth P. Clade-specific differences in neurotoxicity of human immunodeficiency virus-1 B and C Tat of human neurons: significance of dicysteine C30C31 motif. Ann Neurol. 2008; 63:366–376. [PubMed: 18074388]

Mori S, van Zijl PC. Fiber tracking: principles and strategies—a technical review. Biomedicine. 2002; 15:468–480.

Oishi, K., Faria, AV., van Zijl, PC., Mori, S. MRI atlas of human white matter. Academic Press; 2010.

Ortega M, Heaps JM, Joska J, Vaida F, Seedat S, Stein DJ, et al. HIV clades B and C are associated with reduced brain volumetrics. Journal of NeuroVirology. 2013; 19:479–487. [PubMed: 24078556]

Osmanov S, Pattou C, Walker N, Schwardlander B, Esparza J, Isolation W-UNH. et al. Estimated global distribution and regional spread of HIV-1 genetic subtypes in the year 2000. J Acquir Immune Defic Syndr. 2002; 29:184–190. [PubMed: 11832690]

Ostrosky-Solis F, Ramirez M, Ardila A. Effects of culture and education on neuropsychological testing: a preliminary study with indigenous and nonindigenous population. Appl Neuropsychol. 2004; 11:188–195. [PubMed: 15673490]

Paul R, Cohen R, Navia B, Tashima K. Relationships between cognition and structural neuroimaging findings in adults with human immunodeficiency virus type-1. Neurosci Biobehav Rev. 2002; 26:353–359. [PubMed: 12034135]

Paul RH, Ernst T, Brickman AM, Yiannoutsos CT, Tate DF, Cohen RA, et al. Relative sensitivity of magnetic resonance spectroscopy and quantitative magnetic resonance imaging to cognitive function among nondemented individuals infected with HIV. J Int Neuropsychol Soc. 2008; 14:725–733. [PubMed: 18764968]

Paul RH, Joska JA, Woods C, Seedat S, Engelbrecht S, Hoare J, et al. Impact of the HIV Tat C30C31S dicysteine substitution on neuropsychological function in patients with clade C disease. Journal of NeuroVirology. 2014; 20:627–635. [PubMed: 25366660]

Radloff LS. The CES-D scale: a self report depression scale for research in the general population. Applied Psychological Measurements. 1977; 1:385–401.

Ranga U, Shankarappa R, Siddappa NB, Ramakrishna L, Nagendran R, Mahalingam M, et al. Tat protein of human immunodeficiency virus type 1 subtype C strains is a defective chemokine. J Virol. 2004; 78:2586–2590. [PubMed: 14963162]

Rao VR, Sas AR, Eugenin EA, Siddappa NB, Bimonte-Nelson H, Berman JW, et al. HIV-1 clade-specific differences in the induction of neuropathogenesis. J Neurosci. 2008; 28:10010–10016. [PubMed: 18829958]

Rao VR, Neogi U, Talboom JS, Padilla L, Rahman M, Fritz-French C, et al. Clade C HIV-1 isolates circulating in Southern Africa exhibit a greater frequency of dicysteine motif-containing Tat variants than those in Southeast Asia and cause increased neurovirulence. Retrovirology. 2013; 10:61. [PubMed: 23758766]

Rosselli M, Ardila A. The impact of culture and education on non-verbal neuropsychological measurements: a critical review. Brain Cogn. 2003; 52:326–333. [PubMed: 12907177]

Sacktor N, Nakasujja N, Skolasky RL, Rezapour M, Robertson K, Musisi S, et al. HIV subtype D is associated with dementia, compared with subtype A, in immunosuppressed individuals at risk of cognitive impairment in Kampala, Uganda. Clin Infect Dis. 2009; 49:780–786. [PubMed: 19622045]

Sacktor N, Nakasujja N, Redd AD, Manucci J, Laeyendecker O, Wendel SK, et al. HIV subtype is not associated with dementia among individuals with moderate and advanced immunosuppression in Kampala, Uganda. Metab Brain Dis. 2014; 29:261–268. [PubMed: 24515303]

Sheehan DV, Lecrubier Y, Sheehan KH, Amorim P, Janavs J, Weiller E, et al. The mini-international neuropsychiatric interview (M.I.N.I.): the development and validation of a structured diagnostic psychiatric interview for DSM-IV and ICD-10. The Journal of clinical psychiatry. 1998; 59(Suppl 20):22.

Smith SM. Fast robust automated brain extraction. Hum Brain Mapp. 2002; 17:143–155. [PubMed: 12391568]

Stern RA, Silva SG, Chaisson N, Evans DL. Influence of cognitive reserve on neuropsychological functioning in asymptomatic human immunodeficiency virus-1 infection. Arch Neurol. 1996; 53:148–153. [PubMed: 8639064]

Valcour V, Chalermchai T, Sailasuta N, Marovich M, Lerdlum S, Suttichom D, et al. Central nervous system viral invasion and inflammation during acute HIV infection. J Infect Dis. 2012; 206:275–282. [PubMed: 22551810]

Vasan A, Renjifo B, Hertzmark E, Chaplin B, Msamanga G, Essex M, et al. Different rates of disease progression of HIV type 1 infection in Tanzania based on infecting subtype. Clin Infect Dis. 2006; 42:843–852. [PubMed: 16477563]

Yepthomi T, Paul R, Vallabhaneni S, Kumarasamy N, Tate DF, Solomon S, et al. Neurocognitive consequences of HIV in southern India: a preliminary study of clade C virus. J Int Neuropsychol Soc. 2006; 12:424–430. [PubMed: 16903135]

Yushkevich PA, Piven J, Hazlett HC, Smith RG, Ho S, Gee JC, et al. User-guided 3D active contour segmentation of anatomical structures: significantly improved efficiency and reliability. NeuroImage. 2006; 31:1116–1128. [PubMed: 16545965]

Zhang SDC, Laidlaw DH. Visualizing diffusion tensor MR images using streamtubes and streamsurfaces. IEEE Trans Vis Comput Graph. 2003; 9:454–462.

Zhang H, Yushkevich PA, Alexander DC, Gee JC. Deformable registration of diffusion tensor MR images with explicit orientation optimization. Med Image Anal. 2006; 10:764–785. [PubMed: 16899392]

Zhang H, Avants BB, Yushkevich PA, Woo JH, Wang S, McCluskey LF, et al. High-dimensional spatial normalization of diffusion tensor images improves the detection of white matter differences: an example study using amyotrophic lateral sclerosis. IEEE Trans Med Imaging. 2007; 26:1585–1597. [PubMed: 18041273]
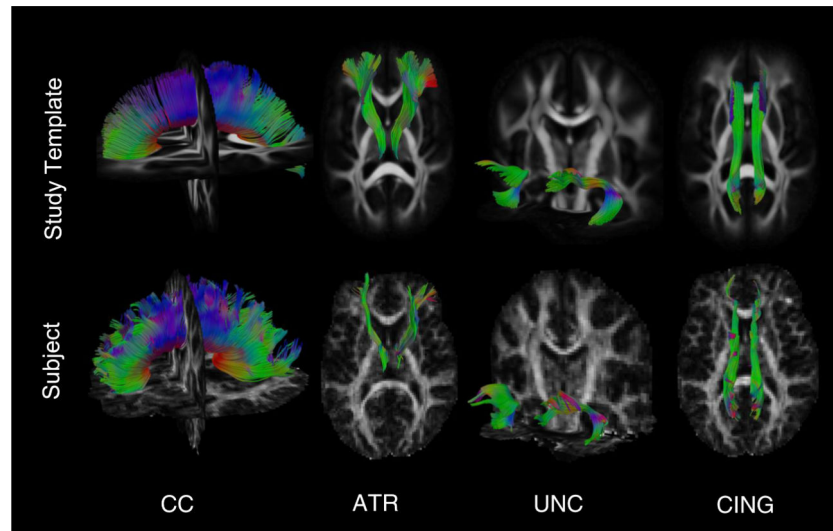
Fig. 1.
Tractography models of white matter tracts derived from diffusion MRI. The *top row* shows tract reconstructions from the study-specific template, and the *bottom row* shows analogous reconstructions from a single subject. The tracts included the corpus callosum (*CC*), anterior thalamic radiation (*ATR*), uncinate fasciculus (*UNC*), and cingulum bundle (*CING*)
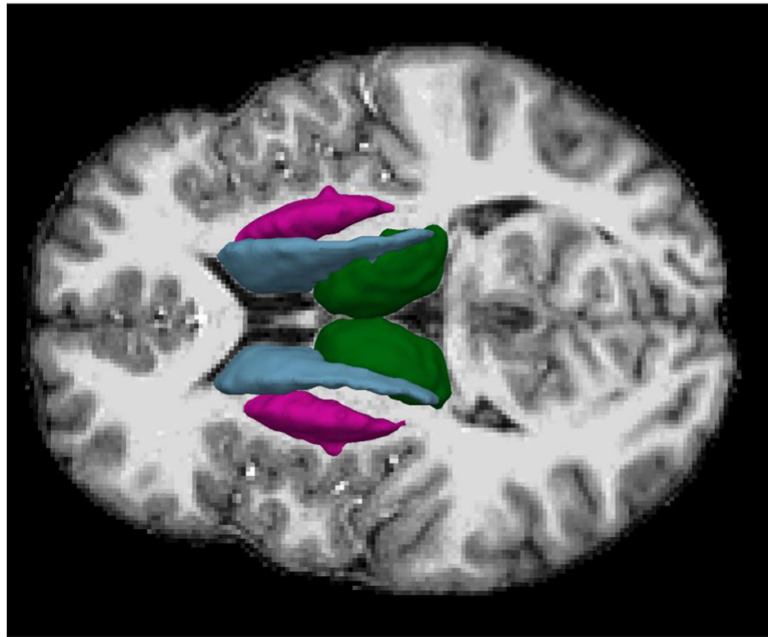
Fig. 2.
Anatomical parcellation of subcortical brain regions derived from T1-weighted MRI. The subcortical structures included the caudate (*blue*), putamen (*pink*), and thalamus (*green*)

Table 1

Demographic characteristics

HIV+ vs. HIV−	HIV+ ($n = 146$)	HIV− ($n = 34$)	p value
Age (years)	31.59 (5.28)	25.41 (4.45)	<0.001
Education (years)	10.22 (1.57)	11.00 (1.63)	0.010
Sex, % female	82.19%	55.88%	0.001
HIV+: C31S vs. C31C	HIV+	HIV+	p value
	C31S ($n = 37$)	C31C ($n = 109$)	
Age (years)	30.67 (4.95)	31.91 (5.38)	0.221
Education (years)	9.92 (1.48)	10.32 (1.59)	0.179
Sex, % female	78.38%	83.49%	0.483
$Log_{10}VL$	4.21 (1.00)	4.17 (1.03)	0.856
CD4 cell count	233.1(121.4)	236.4 (181.5)	0.920
cART treatment, % yes	18.35%	10.8%	0.285
VL_detectable, % yes	100%	97.25%	0.308
Duration (months)	13.41(23.49) ($n = 32$)	11.76(23.13) ($n = 92$)	0.731
CES-D	5.47(3.65) ($n = 32$)	6.19(4.42) ($n = 97$)	0.409

Age, education, $Log_{10}VL$, CD4 cell count, duration of infection, and CESD are reported as mean (SD). Note that sample sizes include any individual with at least one of the two types of imaging data types (DTI metrics or brain volumes) available

Table 2

DTI metrics for HIV+ and HIV− individuals

	HIV+ (*n* = 137) mean (SD)	HIV− (*n* = 24) mean (SD)	Raw *p* value	η^2
FA(×1000)				
CC	0.379(0.024)	0.387(0.018)	0.598	0.002
CING	0.305(0.027)	0.318 (0.022)	0.126	0.015
ATR	0.280(0.017)	0.287(0.015)	0.2818	0.007
UNC	0.252(0.020)	0.276(0.021)	0.0001[*]	0.088
RD(×1000)				
CC	0.557(0.032)	0.534(0.029)	0.023[*]	0.033
CING	0.516(0.031)	0.492 (0.031)	0.008[*]	0.044
ATR	0.552(0.036)	0.522(0.029)	0.0041[*]	0.051
UNC	0.566(0.050)	0.500(0.051)	<.0001[*]	0.140
AD (×1000)				
CC	1.015(0.039)	0.986(0.050)	0.007[*]	0.046
CING	0.823(0.037)	0.800 (0.047)	0.033[*]	0.029

Sample sizes differ from Table 1 as both types of imaging outcomes were not available for all participants

[*] Significant after controlling FDR 0.05

Table 3

Brain volumes among HIV+ and HIV− individuals

	HIV+ (n = 128) mean (SD)	HIV− (n = 29) mean (SD)	Raw p value	η^2
Caudate	7165.83 (863.98)	7774.31 (853.05)	0.019*	0.036
Putamen	10,736.92 (995.45)	11,446.76 (1340.49)	0.035*	0.029
Thalamus	12,580.52 (1192.70)	14,130.59 (1555.16)	<0.0001*	0.123
Corpus callosum	2974.48 (432.35)	3252.31 (514.15)	0.080	0.020
Total white matter	430,769.99 (43,831.29)	466,123.10 (50,324.42)	0.001*	0.067
Total gray matter	564,557.73 (45,700.89)	641,319.52 (41,495.26)	<0.0001*	0.183

Sample sizes differ from Table 1 as both types of imaging outcomes were not available for all participants

*Significant after controlling FDR   0.05

Table 4

DTI metrics for C31S and C31C individuals

	C31S (*n* = 35) mean (SD)	C31C (*n* = 102) mean (SD)	Raw *p* value[+]	η^2
FA				
CC	0.384 (0.026)	0.377(0.023)	0.1447	0.016
CING	0.307 (0.026)	0.305(0.027)	0.6795	0.001
ATR	0.278 (0.017)	0.281(0.017)	0.4500	0.004
UNC	0.254 (0.019)	0.252(0.020)	0.6664	0.001
RD(×1000)				
CC	0.548(0.031)	0.561(0.032)	0.0402	0.031
CING	0.512(0.032)	0.518(0.030)	0.3701	0.006
ATR	0.47(0.036)	0.554(0.036)	0.3049	0.008
UNC	0.563(0.045)	0.567(0.052)	0.7249	0.001
AD (×1000)				
CC	1.006(0.039)	1.017(0.039)	0.1575	0.015
CING	0.818(0.038)	0.825(0.036)	0.3289	0.007

[+]No statistically significant results after controlling FDR 0.05

Table 5

Brain volumes among C31S and C31C individuals

	C31S ($n = 34$) mean (SD)	C31C ($n = 94$) mean (SD)	Raw p value[+]	η^2
Caudate	7297.91 (851.77)	7118.05 (867.89)	0.305	0.008
Putamen	10,951.41 (997.48)	10,659.34 (988.56)	0.143	0.017
Thalamus	12,632.32 (1184.54)	12,561.79 (1201.40)	0.788	0.001
Corpus callosum	2972.62 (308.01)	2975.16(470.75)	0.958	<0.001
Total white matter	435,139.56 (40,428.18)	429,189.51 (45,100.81)	0.505	0.004
Total gray matter	569,544.29 (53,415.77)	562,754.09 (42,747.11)	0.464	0.004

[+]No statistically significant results after controlling FDR 0.05